International Journal of Research and Development in Applied Science and Engineering (IJRDASE)
ISSN: 2454-6844

Design and Analysis of EV Wireless Charging Topology Using LCC Compensation Scheme

Vipin Kumar Shukla[1], Keshav Pratap Yadav[2], Vivek Kushawaha[3]
Electrical Engineering,
R.R. Institute of Modern Technology, U.P., India,
Vp.vipin2911@gmail.com, kpyadav@rrgi.in, vivek941524@gmail.com

Abstract— Remote EV charging is essential because it provides customers with a more practical, reliable, and secure charging solution. A highly efficient remote charging system using a dual-sided LCC compensation topology has been demonstrated; however, a significant drawback is the substantial volume created by the compensation coils. This research proposes an alternative method for integrating the compensation loop into the main coil structure to reduce the system's size. The proposed technique not only reduces the framework's size but also eliminates or minimizes the additional coupling effects caused by the integration to an insignificant level. The remote charging system, with the proposed integration method, can transfer 3.0 kW with 95.5% efficiency at an air gap of 150 mm.

Keywords: AC to DC, EV, WCS, LCC.

1. Introduction:

Electric vehicle (EV) wireless charging system (WCS) has the advantages of convenience, space-saving, etc. So, it has attracted much attention. In recent years, working principle, operation characteristics, system design, and control method of both stationary and dynamic wireless EV charging systems have been studied and applied to some demonstrations [1,2]. In applications of EV wireless charging, rectifier and output filter capacitor are needed to convert the high frequency AC to DC, in order to charge the power battery. Rectifier and the circuit after it are usually equivalent to a pure resistance load to design the system or control strategy [3,4]. A conventional way is using the coefficient $8/\pi2$ to make an equivalent relationship between the rectifier input impedance and the system load resistance [5,6]. However, stray parameters and non-ideal behaviors of the devices will become obvious at the high frequency range [7]. Also, rectifier input impedance can be affected by the input inductance and other parameters. So, it will bring some deviations, if only considering WCS rectifier input impedance as a pure resistance.

Actually, rectifier input impedance of EV wireless charging system contains both resistance part and inductance part [7-9]. It can be expressed as a series of an equivalent resistance and an equivalent inductance [8,9]. Although there has not been an effective method to get the equivalent load impedance of WCS rectifier, some existing researches could be helpful. Based on the on and off states [10], the rectifier and its related inductance and capacitance circuits can be described by the state space model [11], considering the stray resistances and diode forward voltage drop [12]. Then, the expressions of the related voltages and currents have been obtained in the time domain, frequency domain, or complex frequency domain [13,14], which can be used for the analysis of WCS rectifier equivalent load impedance. Besides, non-linear switching functions and circuit simulations could also be adopted to study this issue [15]. The non-linear process of rectifier load will bring some difficulties to system compensation network design. As we know, compensation networks are very important to system performances [16], and can be designed to achieve maximum efficiency, maximum power, or conjugate matching [17,18]. In most cases, a pure resistance is used to express the rectifier load [19]. But the operation modes of WCS rectifier load will affect the working states of compensation network. So, actual equivalent input impedance of WCS rectifier load should be considered, while designing the compensation networks. Load estimation of WCS has faced the same problem.

Effects of the rectifier load could complicate the equations used for load estimation, and lead to the increasing of calculation and control complexity. Hence, a pure resistance load is approximately used for most of the load estimation, detection, or optimal load tracking. Another situation is that the voltages and currents are usually both measured for load estimation, in order to calculate the impedances in the primary side. Since the voltage and current sensors or probes have different phase delays at the high frequency range, some deviations may be introduced into the estimation process. Also, the robustness of the estimation method is very important. It can be analyzed through parameter derivation, root locus, Nyquist curve, Bode graph, or directly calculating the results on conditions of parameter variations. Based on the previous researches, an effective method to quantitatively analyze the equivalent load of WCS rectifier is put forward in the paper firstly. The equivalent load can be independently calculated through the parameters of the rectifier circuit, and the results are basically not affected by other WCS parts. Secondly, a compensation network design method is proposed considering the equivalent impedance of the rectifier load, especially the equivalent inductance. This method will further decouple the primary and secondary side design, to achieve four system performance indicators at the same time. Thirdly, the effects of the rectifier non-linear process are taken into count to estimate the system load resistance. The proposed primary side load estimation method only adopts high

International Journal of Research and Development in Applied Science and Engineering (IJRDASE)
ISSN: 2454-6844

frequency voltages, does not need to measure the currents, and can avoid the phase delay deviations. Also, it does not require wireless communication between the primary and secondary sides.

2. Background:

A meticulous understanding of inductive coupling phenomenon can form the basis of wireless power transfer to electrical and electronic appliances. The utility of resonant magnetic coupling and its theory can provide a deep physical insight into the aspect of designing an effective WPT system with optimum power transfer ability under non ideal charging scenarios. This chapter delineates the background and basic theory related to wireless power transfer. The fundamental mechanism of inductively coupled WPT system as well as resonant inductively coupled WPT system has been sketched out. It reveals the developed resonant WPT system architecture, present research strategy and recent developments. It presents the reported literature about the progress and technology updates of WPT system utilized for practical wireless charging. The consequent applications, deliverables and lack of success of WPTS have been highlighted that necessitates for continued research & developments in this field. After a comprehensive assessment, the inadequacies of the resonant inductively coupled WPT system are outlined to substantiate the direction of the research pursuits of the intended work for EV charging. This would subsequently enable us to deduce operating regime for maximum power transfer of WPT system in order for its widespread adoption for powering as well as charging of Electric Vehicles. The basic knowledge of a resonant inductive link for obtaining both maximum output load power and efficiency has been thrashed out.

In Fabio Corti et. al. (2020) [17] work this paper, the design procedure of an electric vehicle (EV) wireless charger is presented. Unlike most of the systems available in the literature, the proposed charging system is regulated from the vehicle side. The on-board electrical circuit automatically adapts the resonant compensation to guarantee compatibility with the primary inverter characteristics and achieve high transmission efficiency without communication between sides. Moreover, the proposed control strategy, used to regulate the secondary full active rectifier (FAR), allows the supply of the the EV battery, maximizing the efficiency during the whole charging process.

In **Yunhui Wang et. al. (2020) [18]** work, an 11kW wireless charging system based on LCC-SP compensation topology is established, in which a rectifier control with the current doubler is adopted. The impedance characteristics of LCC-SP topology are analyzed. The equivalent impedance of the current doubler is derived by Fourier decomposition of the rectifier current, and then the compensation parameters of LCC-SP are modified according to the derived equivalent circuit. Furtherly, the closed-loop control strategy of the system is proposed by establishing the small-signal model of the current doubler. Simulation and experimental results verified the analysis and validity of the proposed system. Finally, an 11kW wireless charging prototype for electric vehicles is built, and 91.6% efficiency from dc power source to load is achieved.

Development on electric vehicles is becoming an increasingly significant area of focus. It is clear that a lot of study has been done on electric cars, which is why it is essential to continue working on this line of inquiry as the cost of gasoline continues to rise and environmental issues continue to have an impact on the natural world. Within the realm of electric cars, rectifier load-based electric vehicles have earned a significant amount of relevance for wireless charging. Vehicle manufacturers across the board are devoting significant resources to the research and development of electric cars that can be powered by batteries. In most cases, the battery chargers for module electric vehicles are connected to the low-voltage system in order to facilitate the charging process. In **Vineet Kumar Trivedi (2022) [19]** article, a rectifier load is added to an electric vehicle-based wireless charging system, and the fuzzy PI hybrid controller is used to improve the system's power output, efficiency, and other relevant metrics.

3. Methodology:

Full-bridge diode rectifier is the most commonly used topology in EV wireless charging system. Also, dual-side LCC compensation networks can provide several appropriate design degrees of freedom to achieve several system performance indicators at the same time. Moreover, it can be designed to make the system resonant frequency independent of the load condition [16]. So we discuss the rectifier load on the basis of this kind of topology.

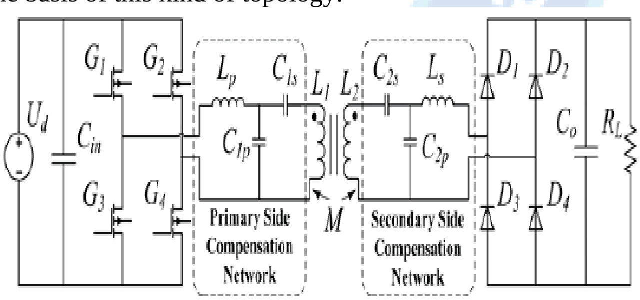

Fig. 1. EV wireless charging system with full-bridge diode rectifier and dual-side LCC compensation networks.

Fig.1 shows the EV wireless charging system with full-bridge diode rectifier and dual-side LCC compensation networks; where, Ud is DC voltage source; the high frequency inverter is composed of G1-G4, and the full-bridge rectifier is composed of D1-D4; the primary side compensation network consists of Lp, C1s, and C1p; the secondary side compensation network consists of Ls, C2s, and C2p; L1 and L2 are self-inductances of the transmit coil and receive coil; M is mutual-inductance

International Journal of Research and Development in Applied Science and Engineering (IJRDASE)
ISSN: 2454-6844

between them; Cin and Co are system input and output filter capacitors; RL is system load resistor. It should be noticed that the WCS load is an EV power battery in the practical case, which behaves as a voltage source series with its parasitic resistance. But the power battery could be equivalent to a load resistance RL [1,19]; the value of this equivalent resistance can be calculated by the voltage on the power battery divided by the current flowing through it. Moreover, the full-bridge rectifier, its input inductor, output filter capacitor, and the load resistor are together defined as the rectifier circuit. Although the following analysis is conducted based on the specific system, it can be extended to applications on other rectifier and compensation network topologies.

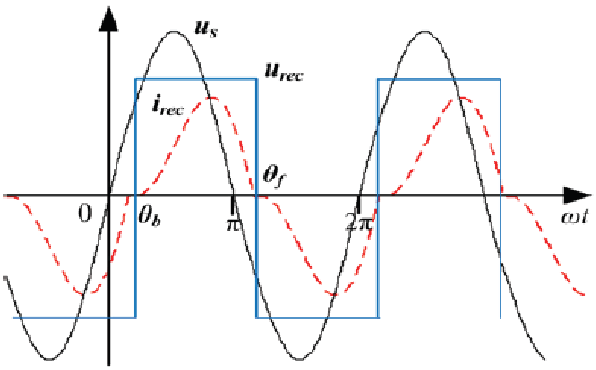

Fig. 2. Schematic waveforms of the source voltage, rectifier input voltage and current.

In order to calculate rectifier equivalent input impedance, we firstly need to analyze the voltages and currents of rectifier circuit, which are shown in Fig.2; where, us is the voltage on C2p, which is a sine wave [18], and can be treated as the voltage source of the rectifier circuit; urec and irec are rectifier input voltage and current; the start time of us positive half-cycle is selected as the coordinate zero of x-axis. θb and θf are start and end phase angles of urec and irec. So, θf =θb+π. Also, the rectifier input inductance Ls should be big enough to keep the rectifier working in the continuous conduction mode (CCM), in order to avoid too large current peaks in the diodes. Hence, only CCM states are shown in Fig.2, and discussed in this paper. Besides, the steady state waveforms of urec and irec are presented in Fig.2, when only a few fluctuations exist on the voltage of the output capacitor Co and the voltage drop on RCo is very small. So, urec can be approximately described as a square wave.

Fig.2 suggests that the waveform of rectifier input current irec has some distortion, because of the effect of the rectifier input inductance. This makes the fundamental wave of irec lags behind the one of urec. So, the rectifier input impedance does not just include resistance component, but also contains a certain inductance component. Moreover, Fig.2 shows that the positive and negative half-cycles are symmetric for all the voltage and current waveforms. Hence, we just need to consider the positive half-cycle, and the negative half-cycle can be obtained from the symmetry. Fig.3 shows the equivalent circuit of the rectifier circuit in the positive half cycle, considering the stray parameters and the diode forward voltage drop; where, udio represents the diode forward voltage drop; Rdio is diode conduction resistance; RLs and RCo are stray resistances of Ls and Co, respectively; ud and id are load voltage and current.

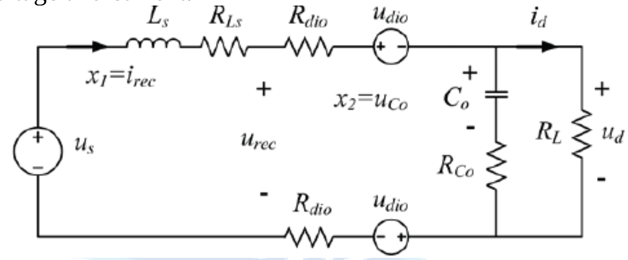

Fig. 3. Equivalent circuit of the rectifier circuit in the positive half cycle.

Based on the equivalent circuit, irec is defined as state variable x1, and the voltage on Co is defined as state variable x2. us and udio are treated as the input variables, and ud is treated as the output variable. So, state space equation of the rectifier circuit in the positive half cycle is given by (1a).

$$\begin{bmatrix} x_1' \\ x_2' \end{bmatrix} = \mathbf{A}\begin{bmatrix} x_1 \\ x_2 \end{bmatrix} + \mathbf{B}\begin{bmatrix} u_s \\ u_{dio} \end{bmatrix}, \quad y = \mathbf{C}\begin{bmatrix} x_1 \\ x_2 \end{bmatrix}$$

Where, impedance matrixes A, B, and C are given by (1b).

$$\mathbf{A} = \begin{bmatrix} -\frac{1}{L_s}(R_{Ls} + 2R_{dio} + \frac{R_L R_{Co}}{R_L + R_{Co}}) & -\frac{1}{L_s}(1 - \frac{R_{Co}}{R_L + R_{Co}}) \\ \frac{R_L}{C_o(R_L + R_{Co})} & -\frac{1}{C_o(R_L + R_{Co})} \end{bmatrix},$$

$$\mathbf{B} = \begin{bmatrix} 1/L_s & -2/L_s \\ 0 & 0 \end{bmatrix}, \quad \mathbf{C} = \begin{bmatrix} \frac{R_L R_{Co}}{R_L + R_{Co}} & 1 - \frac{R_{Co}}{R_L + R_{Co}} \end{bmatrix}.$$

Then, the input variables and the initial values of the state variables are given by (2), according to the schematic waveforms in Fig.2; where, ω is system angle frequency; the diode forward voltage drop is treated as a constant value Vdio. Since only a few fluctuations exist on the voltage of Co and the voltage drop on RCo is very small, their influences can be ignored, and the initial value of x2 can be approximately equivalent to a DC voltage variable Vd. Also, amplitude of us is defined as Vs, and it will be affected by WCS parameters, such as source voltage, mutual-inductance, etc. But the amplitudes of urec and irec are proportional to Vs. So, Vs can be treated as a known variable.

$$u_{s+} = V_s \sin(\omega t + \theta_b), \quad u_{dio} = V_{dio}, \quad \mathbf{x}_+(0) = [0, V_d]^T.$$

Furthermore, Vd and θb should be calculated to solve the state space equation. On the WCS normal working conditions, the value of Vdio and the voltage drops on Rdio and RLs are much smaller than the ones of Vs and Vd. So, the voltage on Ls is approximately equivalent to Vs sinθ - Vd, and the expression of irec can be given by (3), according to the

International Journal of Research and Development in Applied Science and Engineering (IJRDASE)
ISSN: 2454-6844

relationship between the voltage on an inductor and the current flowing through it.

$$i_{rec} = \frac{1}{\omega L_s}\int_{\theta_b}^{\theta}(V_s \sin\theta - V_d)d\theta.$$

As shown in Fig.2, irec=0, when θ=θf=θb+π. So, one relationship between Vd and θb can be got and given by (4).

$$V_d = (2V_s \cos\theta_b)/\pi$$

Also, the DC load current Id can be calculated by (5), which is the average value of id in the positive half cycle.

$$I_d = \frac{1}{\pi\omega L_s}\int_{\theta_b}^{\theta_b+\pi}\int_{\theta_b}^{\theta}(V_s \sin\theta - V_d)d\theta$$

$$= (V_s(2\sin\theta_b + \pi\cos\theta_b) - \pi^2 V_d/2)/\pi\omega L_s.$$

Because Id =Vd /RL, another relationship between Vd and θb can be got and given by (6).

$$V_d = V_s(2\sin\theta_b + \pi\cos\theta_b)/(\pi(\omega L_s/R_L + \pi/2)).$$

Based on the two relationships between Vd and θb, they can be obtained from (4) and (6). The expression of θb is given by (7), and the expression of Vd can also be got according to their relationships. Equation (7) indicates that the phase difference between us and urec (or irec) is mainly decided by Ls and RL, and approximately independent of other WCS parameters. Since amplitudes of urec and irec are basically proportional to the one of us as mentioned above, we can say that the other parts of WCS have little effect on the rectifier circuit, and the rectifier load can be decoupled to analyze its equivalent input impedance. It is should be noticed that the rectifier circuit seems to be equivalent to a pure resistance RL, according to (7). However, this equivalent relationship is only suitable for (7) when calculating the phase angle θb, and cannot be used for any other part in the rectifier load analysis.

$$\theta_b = \arctan(\omega L_s/R_L).$$

After getting Vd and θb, full response of the rectifier circuit in the positive half cycle can be calculated by (8); where, Φ(t) is the characteristic matrix of rectifier circuit; the part before the plus sign is used for solving zero-input response, and the other part is used for solving zero-state response. On the basis of (8), time domain expressions of urec and irec can be obtained, according to the symmetry of their waveforms.

$$\boldsymbol{x}(t) = \Phi(t)\boldsymbol{x}(0) + \int_0^t \Phi(\tau)\mathbf{B}\boldsymbol{u}(t-\tau)\,d\tau$$

$$= e^{\mathbf{A}t}\begin{bmatrix}0\\V_d\end{bmatrix} + \int_0^t e^{\mathbf{A}\tau}\mathbf{B}\begin{bmatrix}V_s\sin(\omega(t-\tau)+\theta_b)\\V_{dio}\end{bmatrix}d\tau.$$

Finally, the fundamental wave amplitudes and phase anglesof u rec and irec can be calculated through Fourier transform, and defined as Urec_fd, Irec_fd, φurec_fd, and φirec_fd. So, the equivalent input impedance of WCS rectifier load will be given by (9); where, Re and Le are series equivalent resistance and inductance of the rectifier load. Only fundamental wave is considered, because the power of the harmonics is much smaller than the one of the fundamental wave. But the harmonic input impedances can also be obtained from Fourier transform.

Moreover, the calculation process suggests Re and Le will be affected by the parameters of the rectifier circuit. Hence, the robustness of this method towards parameter variation needs to be studied. But the theoretical methods, such as calculating the derivative and root locus, cannot provide a simple and clear way to analyze the robustness in this case, since it is related to some complex or non-linear operations.

$$R_e = (U_{rec\_fd}/I_{rec\_fd})\cos(\varphi_{urec\_fd} - \varphi_{irec\_fd}),$$

$$L_e = (U_{rec\_fd}/I_{rec\_fd})\sin(\varphi_{urec\_fd} - \varphi_{irec\_fd})/\omega.$$

To sum up, the above analysis suggests that the rectifier load equivalent impedance contains both resistance and inductance components. Also, the series equivalent resistance and inductance can be independently calculated through parameters of rectifier circuit, and the results are basically not affected by other WCS parameters. So, the rectifier load can be decoupled with other parts of WCS, and make system design easier.

4. Results and Discussions:

Fig. 4 displays all of the preliminary results. The exploratory outcome when the system is completely altered is shown by the solid line in Fig. 4 (a). The structure efficiency is at its peak at the most outrageous outcome power, and it exhibits fantastic consistency with the duplicated efficiency twist in Fig. 3.2. The assessment on Z-bearing misalignment's delayed effect is shown on the scrambling spot line. When the air aperture is increased to 200 mm, the system can move 1.76 kW with a sufficiency of 94.4%. The system execution on X-heading misalignment is shown by the concrete line with circles. When the X-heading misalignment increases by 100 mm, the system transmits 1.57 kW of power with a sufficiency of 93.8%. The show is a little more defenceless as a result, Since the driver can change more easily when the car is left, it is categorically recommended to align the X bearing with the front-back heading of the vehicle. The ran and specked lines display the Y-bearing structural execution. The structure performs significantly improved in this way. Even when the misalignment increases by 150 mm, the structure can still transmit about 2.0 kW with a 94.8% efficiency. Since it can be difficult for drivers to change when the vehicle is left, this heading should be door to door. Fig. 4(a) demonstrates that the outcome power decreases by 33.33% from the best outcome power in Y-bearing, 41.33% in Z-course, and 47.69% in X-heading when misalignment all over occurs. The reason for this is illustrated by (15), which demonstrates how the fundamental coupling coefficient k decays while other portion considerations remain essentially identical. Figure 4(b) illustrates how misalignment causes the conscious primary coupling coefficient k to decrease. When the misalignment increases to 150 mm in the Y-course, k drops to 0.1244, or 33.72% less than its exceptional value (k = 0.1877); when it increases to 50 mm in the Z-bearing, k drops to 0.1045, or 44.33% less; and when it increases to 100 mm in the X-course,

International Journal of Research and Development in Applied Science and Engineering (IJRDASE)
ISSN: 2454-6844

k drops to 0.1, or 46.72% less. When there is misalignment, the differences in inductance values are what achieve the qualifications in the various lost rates between the outcome power and the major coupling coefficient. However, the differences are within 3%, indicating that the fundamental views barely alter. How the efficiency varies as there are misalignments everywhere is seen in Fig. 4(c). By pure coincidence, efficiency declines as misalignment rises. Additionally, the central coupling coefficient twist in Fig. 4(b) and the capacity twist in Fig. 4(c) exhibit truly remarkable consistency. Trial results show that the remote accusing arrangement of the new joining strategy not only benefits from the dual advantages of conservatism and high productivity, but also eliminates the additional coupling impacts or limits them to a negligible level, which significantly enhances the framework investigation and plan.

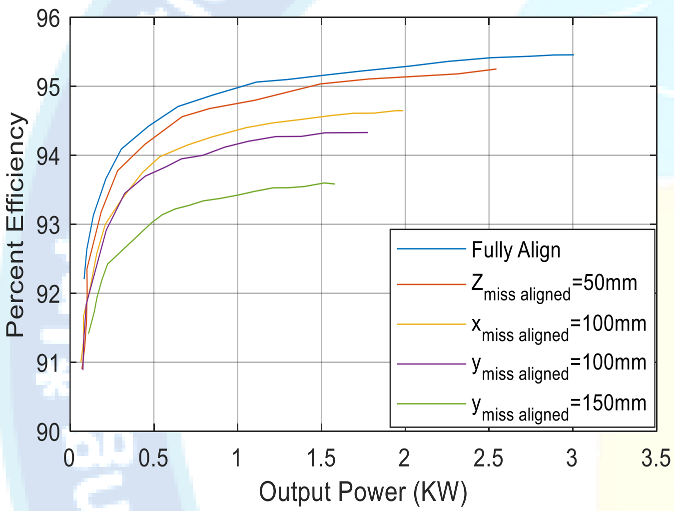

Figure 4: Variation of percentage Efficiency with respect to output power (KW).

5. Conclusion:

This paper gives another incorporated strategy for a remote charging framework utilizing twofold sided LCC remuneration geography. With the remunerated curls incorporated into the primary loop structure, the framework turns out to be significantly more minimized. The proposed remunerated curl configuration further kill or limit the additional coupling impacts to an insignificant level, making it more direct to plan a remote charging framework utilizing the twofold sided LCC pay geography. The definite plan methods to further develop framework proficiency are additionally presented. Both the reproduction results and the hypothetical outcomes confirm the proposed thought. The conservative and exceptionally productive remote charging framework can convey 3.0 kW at a dc proficiency of 95.5% with an air hole of 150 mm when completely adjusted. Our potential work is to introduce the planned remote charger on a vehicle. That's what to accomplish, we won't just examine the extra power misfortune came about because of encompassing items, for example, the EV skeleton and the prepares covered in the ground, yet in addition improve the ferrite plates so least ferrite bars are utilized to convey a similar measure of influence with serious proficiency

References:

[1] S. Q. Li, and C. C. Mi, “Wireless power transfer for electric vehicle applications,” IEEE J. Emerg. Sel. Topics Power Electron., vol. 3, no. 1, pp. 4-17, Mar. 2015.
[2] Y. D. Ko, and Y. J. Jang, “The optimal system design of the online electric vehicle utilizing wireless power transmission technology,” IEEE Trans. Intell. Transp. Syst., vol. 14, no. 3, pp. 1255-1265, Sep. 2013.
[3] W. X. Zhong, and S. Y. R. Hui, “Maximum energy efficiency tracking for wireless power transfer systems,” IEEE Trans. Power Electron., vol. 30, no. 7, pp. 4025-4034, Jul. 2015.
[4] D. Ahn, S. Kim, J. Moon, and I. K. Cho, “Wireless power transfer with automatic feedback control of load resistance transformation,” IEEE Trans. Power Electron., vol. 31, no. 11, pp. 7876-7886, Nov. 2016.
[5] M. P. Theodoridis, “Effective capacitive power transfer,” IEEE Trans. Power Electron., vol. 27, no. 12, pp. 4906-4913, Dec. 2012.
[6] D. Thenathayalan, and J. H. Park, “Wide-air-gap transformer model for the design-oriented analysis of contactless power converters,” IEEE Trans. Ind. Electron., vol. 62, no. 10, pp. 6345-6359, Oct. 2015.
[7] M. Fu, Z. Tang, M. Liu, C. Ma, and X. Zhu, “Full-bridge rectifier input reactance compensation in megahertz wireless power transfer systems,” in Proc. 2015 WoW, 2015, pp. 1-5.
[8] A. Berger, M. Agostinelli, S. Vesti, J. A. Oliver, J. A. Cobos, and M. Huemer, “A wireless charging system applying phase-shift and amplitude control to maximize efficiency and extractable power,” IEEE Trans. Power Electron., vol. 30, no. 11, pp. 6338-6348, Nov. 2015.
[9] K. Colak, E. Asa, M. Bojarski, D. Czarkowski, and O. C. Onar, “A novel phase-shift control of semibridgeless active rectifier for wireless power transfer,” IEEE Trans. Power Electron., vol. 30, no. 11, pp. 6288-6297, Nov. 2015.
[10] Y. Akihara, T. Hirose, S. Masuda, N. Kuroki, M. Numa, and M. Hashimoto, “Analytical study of rectifier circuit for wireless power transfer systems,” in Proc. ISAP, 2016, pp. 338-339.
[11] H. C. Li, K. P. Wang, L. Huang, W. J. Chen, and X. Yang, “Dynamic modeling based on coupled modes for wireless power transfer systems,” IEEE Trans. Power Electron., vol. 30, no. 11, pp. 6245-6253, Nov. 2015.
[12] S. Aldhaher, P. C. K. Luk, K. E. K. Drissi, and J. F. Whidborne, “High-input-voltage high-frequency class E rectifiers for resonant inductive links,” IEEE Trans. Power Electron., vol. 30, no. 3, pp. 1328-1335, Mar. 2015.
[13] H. T. Shi, J. D. Mao, X. S. Li, and J. T. Pan, “Modeling and analysis of impedance for uncontrolled rectifier based nonlinear load,” in Proc. CCDC, 2016, pp. 1770-1775.
[14] C. K. Lee, S. Kiratipongvoot, and S. C. Tan, “High-frequency-fed unity power-factor AC-DC power converter

ISSN: 2454-6844

with one switching per cycle," IEEE Trans. Power Electron., vol. 30, no. 4, pp. 2148-2156, Apr. 2015.

[15] Q. Lei, M. Shen, V. Blasko, and F. Z. Peng, "A generalized input impedance model of three phase diode rectifier," in Proc. APEC, 2013, pp. 2655-2661.

[16] S. Q. Li, W. H. Li, J. J. Deng, T. D. Nguyen, and C. C. Mi, "A double-sided LCC compensation network and its tuning method for wireless power transfer," IEEE Trans. Veh. Technol., vol. 64, no. 6, pp. 2261-2273, Jun. 2015.

[17] Corti, Fabio, et al. "A secondary-side controlled electric vehicle wireless charger." Energies 13.24 (2020): 6527.

[18] Wang, Yunhui, et al. "Research on 11kW wireless charging system for electric vehicle based on LCC-SP topology and current doubler." 2020 IEEE Energy Conversion Congress and Exposition (ECCE). IEEE, 2020.

[19] Trivedi, Vineet Kumar. "Electric Vehicle Charging System with Rectifier Load using Hybrid Fuzzy-PI Controller." International Journal of Innovative Science and Research Technology, Volume 7, Issue 6, June – 2022.

[20] Kushawaha, Vivek, Gaurav Gupta, and Lalit Singh. "Enhancing Energy Efficiency: Advances in Smart Grid Optimization." International Journal of Innovative Research in Engineering and Management 11.2 (2024): 100-105.

[21] Yadav, Nitya, Ramendra Tripathi, and Vivek Kushawah. "Charging Ahead-Addressing Key Barriers to Electric Vehicle Market Penetration in India." International Journal of Innovative Research in Computer Science & Technology 12.3 (2024): 45-50.

[22] Kushawaha, Vivek, et al. "ENHANCEMENT OF VOLTAGE PROFILE IN TRANSMISSION LINE USING DSTATCOM AND DVR." International Journal of Advanced Computer Technology 10.6 (2021): 01-05.

[23] Kushwaha, Vivek, and Asif Ali. "Environmental, Techno-Economic Feasibility Analysis of Grid-Connected Photovoltaic Power Plants in Subtropical Region." International Journal of Research and Development in Applied Science and Engineering 23.1 (2023).

[24] Vivek Kushwaha, Dharmendra Yadav, Ashish Mishra, "Techno-Economic Feasibility Analysis of Grid-Connected Photovoltaic Power Plants", IJRAR - International Journal of Research and Analytical Reviews (IJRAR), E-ISSN 2348-1269, P- ISSN 2349-5138, Volume.11, Issue 2, Page No pp.778-782, May 2024, Available at : http://www.ijrar.org/IJRAR24B3436.pdf